Author(s):   Simppa Äkäslompolo, Taina Kurki-Suonio, Otto Asunta, Mario Cavinato, Mario Gagliardi, Eero Hirvijoki, Gabriella Saibene, Seppo Sipilä, Antti Snicker, Konsta Särkimäki, and Jari Varje

Title: ITER fast ion confinement in the presence of the European test blanket module

ITER fast ion confinement in the presence of the European test blanket module

Simppa Äkäslompolo[1]**, Taina Kurki-Suonio**[1]**, Otto Asunta**[1]**,
Mario Cavinato**[2]**, Mario Gagliardi**[2]**, Eero Hirvijoki**[1]**, Gabriella Saibene**[2]**,
Seppo Sipilä**[1]**, Antti Snicker**[1]**, Konsta Särkimäki**[1] **and Jari Varje**[1]

[1] Department of Applied Physics, Aalto University, FI-00076 AALTO, Finland
[2] Fusion for Energy, Torres Diagonal Litoral, Edificio B3, 08019 Barcelona, Spain

E-mail: simppa.akaslompolo@alumni.aalto.fi

Abstract

This paper addresses the confinement of thermonuclear alpha particles and neutral beam injected deuterons in the *15 MA Q = 10 inductive scenario* in the presence of the magnetic perturbation caused by the helium cooled pebble bed test blanket module using the vacuum approximation. Both the flat top phase and plasma ramp-up are studied. The transport of fast ions is calculated using the Monte Carlo guiding center orbit-following code ASCOT.
A detailed three-dimensional wall, derived from the ITER blanket module CAD data, is used for evaluating the fast ion wall loads. The effect of the test blanket module is studied for both overall confinement and possible hot spots. The study indicates that the test blanket modules do not significantly deteriorate the fast ion confinement.

Keywords: ITER, fast ions, test blanket module, wall loads, orbit following, Monte Carlo

S Online supplementary data available from stacks.iop.org/NF/55/093010/mmedia

(Some figures may appear in colour only in the online journal)

1. Introduction

While the fusion reactor ITER is built in order to demonstrate the technological and scientific feasibility of fusion energy, it also serves as a test bed for components of DEMO, the next reactor that will demonstrate, e.g. the large-scale production of electrical power and tritium fuel self-sufficiency. In particular, ITER test blanket modules (TBMs) will test the technology of tritium breeding modules for DEMO. Three equatorial ports are reserved for the modules in ITER.

The DEMO designs use ferritic steel [1]. Hence ferromagnetic material will be used also for the ITER TBMs. The problem with ferromagnetic components is that in the strong magnetic field of a tokamak they get magnetized and produce an additional field. Such local perturbations, like any deviation from the axisymmetric magnetic field, compromise the conservation of the toroidal canonical momentum and the closure of the guiding-centre orbits in the poloidal plane. Thus, in the presence of ferromagnetic TBMs, the magnetic field may be less efficient in confining the plasma. The weakly collisional

energetic ions are especially susceptible for changes in the magnetic field structure and may even be channelled out of the plasma by malignant perturbations. This could result in hot spots on the first wall [2].

In this article we investigate whether the helium-cooled pebble bed TBM, the heaviest of the European TBM designs, jeopardises the confinement of energetic ions in ITER. To this end, we perform particle simulations of various fast ion species for the ITER deuterium–tritium phase *15 MA Q = 10 inductive scenario* using the ASCOT [3] suite of codes. It has been previously used for predicting ITER [4, 5] wall loads as well as simulating the TBM mock-up experiments at DIII-D [6]. Other ITER TBM designs have been studied by others [7–9].

Both alpha particles born in thermonuclear reactions and deuterons from neutral beam injection (NBI) are followed until collisions with the thermal plasma have slowed them down to either twice the local thermal energy or, if the local temperature is below 5 keV, to 10 keV. Both the 3D magnetic field and wall model have been constructed from CAD drawings,

imported from the ITER database in 2013. Altogether eight cases are addressed: the two particle species are simulated with and without the perturbation due to the TBMs, and the analyses are carried out for two different phases of the ITER discharge. One time slice is from the ramp-up (RU) phase at 60 s and the other corresponds to the flat top (FT) phase at 470 s. In the RU phase the plasma current has reached approximately 80% of the flat top value. In all simulations, the effect of the ferritic inserts [10, 11] mitigating the toroidal field coil ripple is included.

The structure of this article is as follows: In section 2, the numerical model and the inputs are described. The simulations results are presented in section 3, where it is shown that the TBMs have only a small effect on fast ion confinement. Finally, in section 4, we discuss the results, including possible caveats and topics for future work.

## 2. Description of input data and the model

The overall simulation scheme is to follow the motion of fast ions in a precalculated plasma and magnetic background while they are slowing down. Within this study, we are mostly interested in the statistics, power deposition in particular, of particles that hit the first wall.

2.1. Test particle following

The ASCOT code [3] follows the guiding centres of charged particles in the 3D magnetic fields of a tokamak. The guiding-center approach is reasonable when none of the background parameters changes appreciably over a gyro-orbit. This requirement is fulfilled for both fusion alphas and NBI deuterons in ITER: the gyro radii of the alpha particles can reach ∼7 cm, while the gradient lengths are of the order of a few meters. However, it should be noted that, in non-axisymmetric configuration, there can exist gyro-orbit transport mechanisms that are not captured by the guiding centre formalism [12]. While a small-scale study of such effects suggests that they do increase the fast ion wall loads somewhat [13], the computing time requirement of full gyro-motion simulations keeping reasonable statistics would be prohibitive.

The Coulomb interaction with the background plasma, leading to slowing-down and transport of the energetic ions, is modeled with Fokker–Planck collision operators (equations (54)–(56) in [14]). The particles are followed until they either intersect the first wall or are thermalized. Therefore the simulation setup consists of the *static* one-dimensional plasma profiles, two-dimensional plasma equilibrium and three-dimensional magnetic field. The particle orbits are bound by a three-dimensional wall.

While the bulk simulation is carried out following only the guiding centers, once the ion approaches any plasma-facing component the full orbit following is adopted to accurately determine the location of the impact. Since the gyro-phase information is lost in the guiding center formalism, a random phase is given to a particle each time full gyro motion following is initiated. This 'hybrid' approach improves the
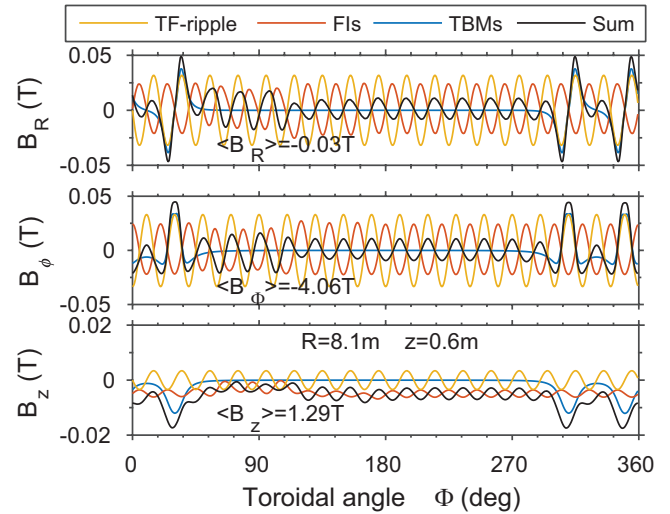

Figure 1. The non-axisymmetric component of the magnetic field values as a function of the toroidal angle. The data is shown for the flat top phase at a single poloidal location at magnetic midplane with $\rho_{pol} = 0.95$. The toroidal mean value is indicated for each component.

reliability of the results by not missing impacts along the gyro orbit but keeps the computing time reasonable compared to pure full-orbit simulation. If the ion does not reach the wall but starts receding from it, the full orbit is dropped and only the guiding center that has been advanced in parallel with the full orbit, is followed further.

The ASCOT simulations are carried out assuming a steady state, which is easily justified for the flat top. In the ramp-up phase, this is justified because of the slow ramp-up rate used in ITER. The plasma current (and other quantities) change by approximately 1.3% per second, while in the simulations the particles slow down in less than 1.5 s.

2.2. Magnetic and plasma backgrounds and the three-dimensional wall

The magnetic field has the following non-axisymmetric features, in decreasing order of mean amplitude: (i) ripple caused by the 18 toroidal field (TF) coils, (ii) the field due to the magnetized ferritic inserts (FIs) that cancel much of the TF coil ripple, and (iii) the field due to the magnetized TBMs. The field amplitudes for the flat top phase as a function of the toroidal angle at a constant poloidal location are shown in figure 1. The TF coil ripple field is reproduced by directly integrating the Biot–Savart law for the detailed full TF-coil winding with 134 turns [15]. Calculating the field due to the magnetization of the ferromagnetic components requires a more complex procedure utilizing the finite element method (FEM) with non-linear magnetic material properties for the ferromagnetic components [16]. In the 3D magnetic field, it is assumed that all six ITER TBMs (two in each of the three dedicated ports) are of the European helium cooled pebble bed type. The magnetizing field is calculated using the geometry of the TF and poloidal field (PF) coils, together with the plasma current from the equilibrium. The three-dimensional magnetic field obtained this way (figure 2) is tabulated into a
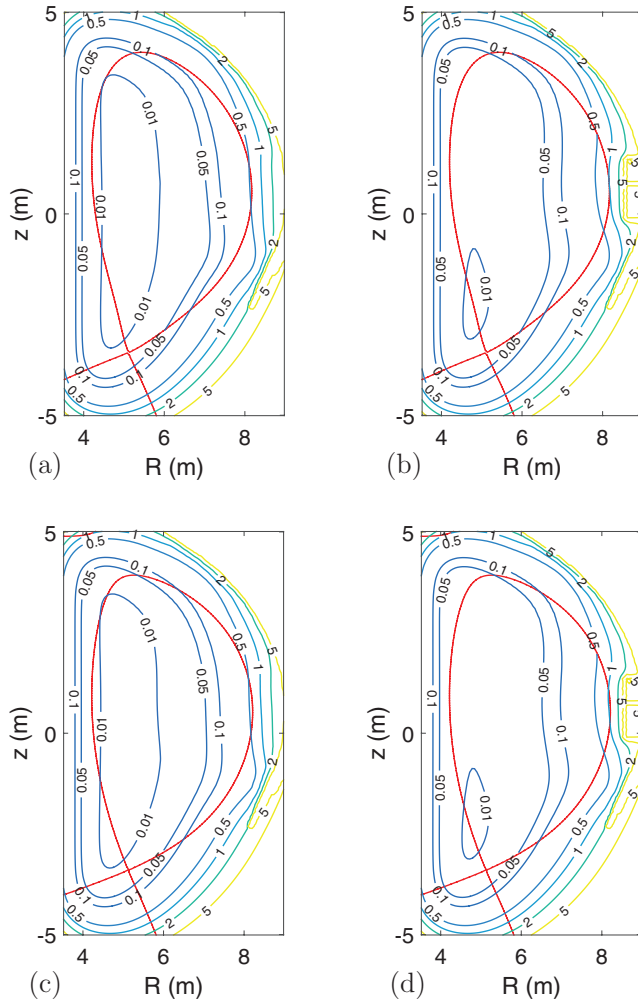
Figure 2. The effective 'ripple' maps, giving a measure of how much the toroidal field strength varies at a given point in the poloidal plane when going around toroidally for the different simulated cases: panels (*a*) and (*b*) show the flat top phase and (*c*) and (*d*) show the ramp-up phase. The TBMs are present in panels (*b*) and (*d*). The actual expression is $100 \times \left[\max(B_\phi) - \min(B_\phi) \right] / \left[\max(B_\phi) + \min(B_\phi) \right]$, thus the ripple is given in percents. Thus the numbers on the contours give the maximum of any local perturbation of the toroidal field, not the amplitude of any periodic 'ripple'. The overall shape results from the D-shape of the toroidal field coils. The plots show clearly the location of the TBMs at the LFS midplane and the shape of the FIs at the 5% contour. The TBMs push the 0.01% contour into a small area below the midplane. See the supplementary material (stacks. iop.org/NF/55/093010/mmedia) for Poincaré plots of the magnetic fields.

rectangular grid in cylindrical coordinates, with 92 radial, 168 vertical and 540 toroidal points. The fields are evaluated at required locations with spline interpolation. Finally, the field due to the two-dimensional equilibrium, (described below), is added.

In this study, the vacuum field approach is used. Including the plasma response to the non-axisymmetric vacuum field would require using advanced MHD codes, such as MARS-F [17] or JOREK [18]. However, since it is the plasma rotation that affects the plasma response and ITER plasmas are

expected to exhibit only slow rotation, using the vacuum approach is a reasonable first approximation, corresponding to slowly rotating ITER plasmas.

A combination of 1.5D transport codes and free-boundary equilibrium codes [19] were used to self-consistently calculate the plasma profiles (figure 3) and the equilibrium (figure 4). As the radial coordinate, ASCOT uses ρ_{pol} calculated from the poloidal flux ψ and its values at the plasma separatrix $\psi_{separatrix}$ and at the magnetic axis ψ_{axis}: $\rho_{pol} = \sqrt{(\psi - \psi_{axis})/(\psi_{separatrix} - \psi_{axis})}$. The mapping between ρ_{pol} and the major radius R along the midplane at the low-field side is shown along with the profiles in figure 3. The local values of plasma parameters (electron and ion temperatures and densities) needed for the collision operators are evaluated from the corresponding 1D profiles using ρ_{pol} calculated from the axisymmetric equilibrium.

The three-dimensional first wall geometry was obtained from the configuration model of the blanket modules and from simple models of the port plugs [15, 20]. Ray tracing and defeaturing tools produced a triangulation of the plasma facing components with 339 840 triangles of approximately 25 cm^2 mean (and median) surface area [21]. A 3D view of the wall is shown in figure 5.

2.3. Test particle generation

ASCOT features *ab initio* models for both thermonuclear fusion alphas and the NBI ions from ITER heating beams, while a comprehensive study of energetic ions generated by ion cyclotron resonance heating (ICRH) awaits the proper *ab initio* model.

Test particles corresponding to the 3.5 MeV alpha particles are initialized uniformly in Cartesian coordinates filling the plasma volume. Due to the toroidal geometry of the plasma, this initialization places fewer test particles at the high field side than on the interesting low field side, where the magnetic perturbations are strongest. Each particle is assigned a weight factor corresponding to the local D–T fusion reactivity calculated from the density and temperature profiles according to Maxwellian reactivity given in [22]. The alpha particles have an isotropic velocity distribution and the proper Maxwellian energy distribution around 3.5 MeV [23].

Besides thermonuclear D–T fusion, there are also other sources of fusion products: beam-target and beam–beam fusion reactions await implementation of the anisotropic initial energy distribution. Also thermonuclear reactions between deuterons are omitted. However, as will be shown below, these unaccounted-for fusion products carry less than three percent of the power of the thermonuclear alphas.

The test particle population corresponding to neutral beam injection is generated using the beamlet-based neutral beam injection code BBNBI [24]. The 1 MeV neutral particles are traced from the injector into the plasma and, at each step, their ionization probability is evaluated using total ionization cross section from [25]. Once the accumulated probability exceeds a pre-determined, test particle-specific threshold, a new NBI ion is generated in the plasma. Consequently, the
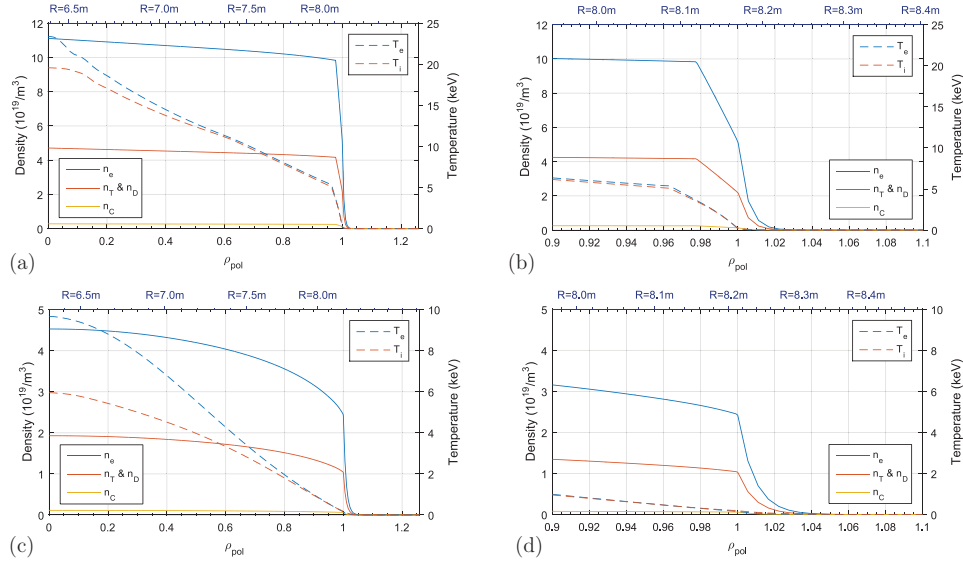
Figure 3. The plasma profiles for the flat top (*a*) and (*b*) and ramp-up (*c*) and (*d*) phases. Figures (*b*) and (*d*) are close-ups on the pedestal and scrape-off layer profiles as a function of ρ_{pol}. The corresponding values of the major radius R at the outer midplane are shown at the top of each plot. The plasma consists of bulk deuterium $_D$ and tritium $_T$ with identical densities n, and carbon $_C$ as impurity. All the ion species are assumed to have the same temperature T_i, but distinct from the electron temperature T_e. (Note: the transport calculations were made before the decision to have a full metal ITER. Therefore carbon is used as the main impurity here. Tests with tungsten impurity instead of carbon have been carried out, but no significant changes in the results were found.)
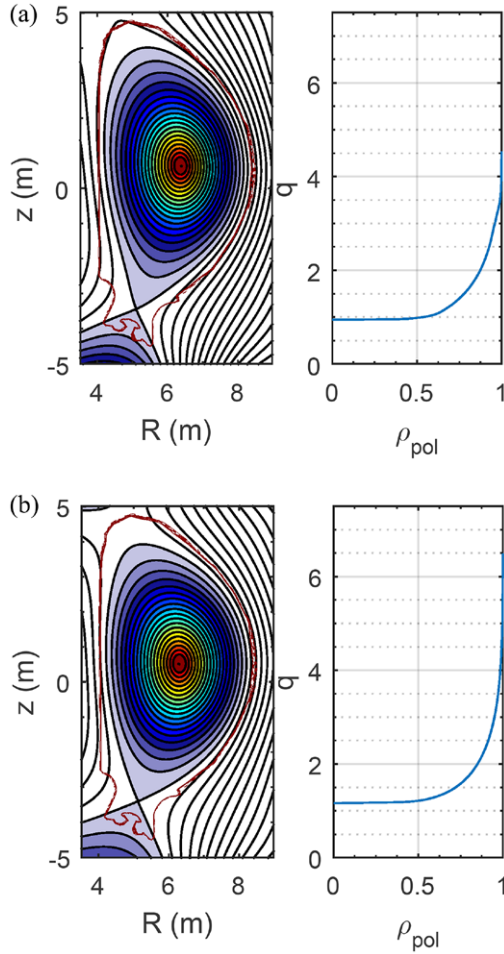
Figure 4. The plasma equilibrium and safety factor q profile for the flat top (*a*) and ramp-up (*b*) phases. The contours show the flux surface label ρ_{pol} with 0.05 increment. A sketch of the poloidal projection of the 3D wall is also included.

spatial distribution of the NBI ions is directly mapped into an ensemble of test particles with equal weight factors.

3. Confinement analysis from slowing-down simulation results

The goal of the ASCOT simulations is to assess if and how the TBMs affect the fast ion confinement. This is accomplished by carrying out pairs of simulations where the only difference between the two is the absence or presence of the TBMs. The simulations are carried out assuming that the plasma is MHD-quiescent and that any microturbulence present in the plasma is not affecting high-energy ions.

3.1. Initial test particle ensemble

In the alpha particle simulations, the thermonuclear alpha power from deuterium–tritium reactions was calculated to be 85 MW in the FT phase and 430 kW in the RU phase. In the FT phase, the thermonuclear alphas carry 97.2% of the fusion power going to charged particles. Alphas from the beam-target reactions carry 2.6%. The protons from deuterium–deuterium reactions carry 0.34% while the ^{3}He ions carry 0.1% of the power. Though we can calculate the reactivity for all the reactions, the anisotropic birth distribution has not yet been implemented in our tools. Hence, only the thermonuclear alphas are considered in this study.

In the case of the beam ions, the total NBI power was set to 33 MW. In ITER, there are two neutral beam boxes. The beams can be tilted vertically to move the deposition on-axis or off-axis. All injection geometries were included in the simulations by assigning one fourth of the test particles to each of four 8.25 MW beams. In the FT phase, the shine-through fraction was 0.030%, and for the RU phase it was about 2.8%.
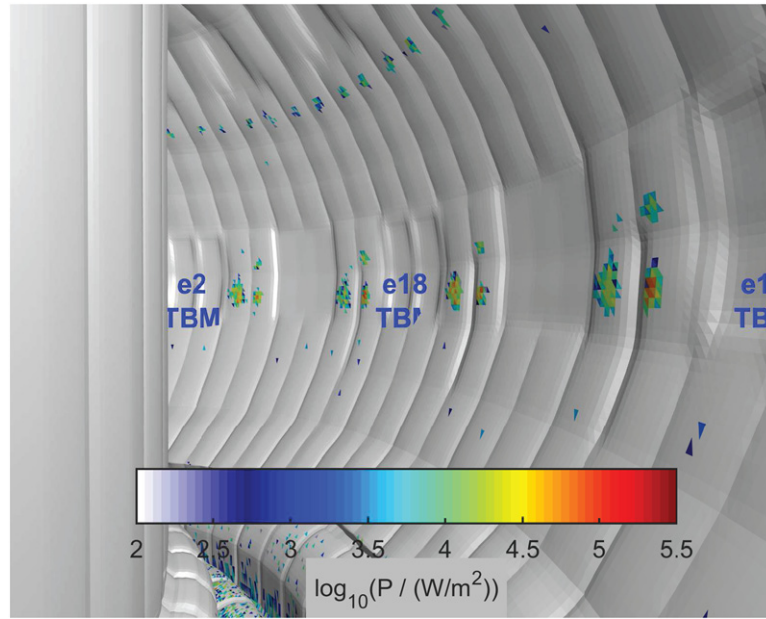
Figure 5. The 3D wall with power load due to thermonuclear alphas for the flat top phase in the presence of the TBMs. Most of the wall hits are at the slightly protruding parts of the first wall blanket. The TBMs are recessed, and receive no direct fast particle hits.
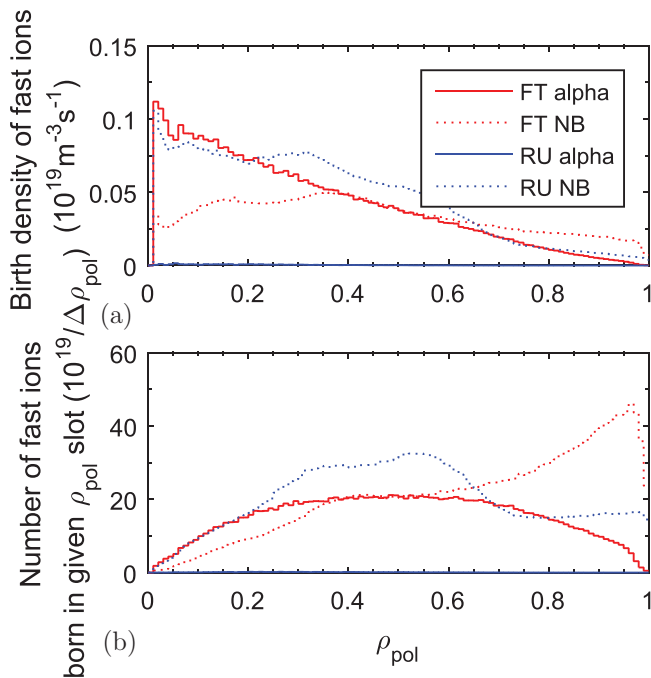
Figure 6. The particle loading as a function of the minor radius coordinate ρ_{pol}. The data is presented both (*a*) as flux surface averaged density and (*b*) as the pure number of particles born in each rho slot.

This results in over 1 MW m^{-2} wall power load from the neutral deuterium hitting the wall in RU phase. This should be compared to the maximum design load for the first wall, 2–5 MW m^{-2}. Therefore, reduced beam power in the RU phase might be in order.

In each simulation, the test particle ensemble consists of a million test particles, except for the very few alphas born in RU phase which is analyzed with only 10 000 test particles. The radial profiles of the birth density are shown in figure 6(*a*). To illustrate the actual abundance of fast ions in

different parts of the plasma, the number of ions born in a given ρ_{pol} slot is also shown in figure 6(*b*). The birth distributions of particles, both in configuration and velocity space, are illustrated in figures 7–9.

3.2. Wall power loads and slowing-down distributions

The total power loads to the ITER first wall are given in table 1 for the eight cases studied. The table differentiates between power deposited to the first wall and power heating the divertor. The numbers are very small, measured in tens of kW, but they clearly show an increase in wall loads when the TBMs are introduced. However, even if the losses are doubled or tripled, they remain very small.

Comparing the loads of different phases in the discharge, one notices that the wall loads from NBI in the RU phase are even smaller than those in the FT phase. This is attributed to the lower plasma density during RU, causing the bulk of NBI ionization to occur deep in the plasma core and mainly onto passing orbits. However, as already mentioned, while the power loads due to *charged* particles from NBI are minuscule, the shine-through in the RU phase is alarmingly large. Therefore it can be concluded that, in this phase, the wall protection should concentrate on neutral particles passing through the plasma. In the FT phase, a measurable fraction of ions are born on banana orbits in the perturbed edge region, see figures 7 and 9. The TBMs cause deuterons to be transported out from slightly deeper ($\rho_{pol} = 0.81$ versus $\rho_{pol} = 0.86$) and, for NBI deuterons born at the edge, increase the probability of being lost from 0.3% to 0.7%. The total fraction of NBI deuterons lost to the wall increases from 67×10^{-5} to 170×10^{-5}, thus increasing the wall losses.

The losses of fusion alphas are an order of magnitude higher than those of beam injected ions, which is readily understood from their birth profiles in the velocity space: the

Table 1. Comparison of wall and divertor power loads with and without the TBMs for the two phases (RU and FT) of the ITER 15 MA scenario.

		Wall		Divertor	
		FT	RU	FT	RU
alpha	without TBM	35 ± 1 kW	< 0.1 kW	127 ± 1 kW	< 0.1 kW
	with TBM	68 ± 1 kW	< 0.1 kW	127 ± 1 kW	< 0.1 kW
NBI	without TBM	1.7 ± 0.1 kW	< 0.1 kW	0.9 ± 0.9 kW	1.1 ± 1.1 kW
	with TBM	6.9 ± 0.2 kW	< 0.1 kW	0.9 ± 0.9 kW	< 0.1 kW
NBI shine-through		9.9 kW	926 kW	< 0.1 kW	< 0.1 kW

Note: The uncertainty estimates are calculated from 50 bootstrap samples. Also the shine-through of NBI neutrals is included since it was found important in some cases. In the model, the presence of TBMs does not affect the shine-through.
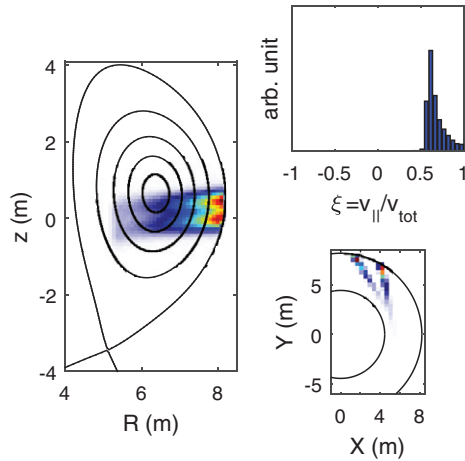
Figure 7. The initial test particle distribution of neutral beam injected deuterons in the **flat top** phase. The distribution includes both heating beams in both on- and off-axis orientation. All NBI deuterons have 1.0 MeV initial energy.
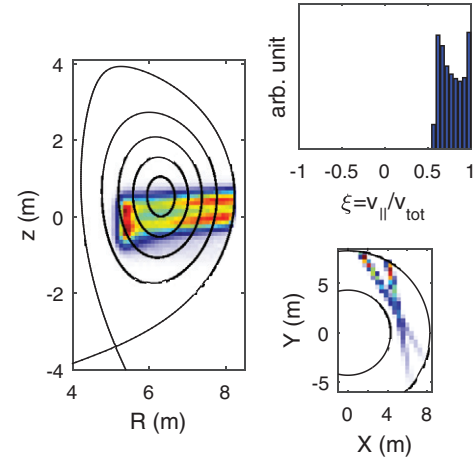
Figure 9. The initial test particle distribution of neutral beam injected deuterons in the **ramp-up** phase. The distribution includes both heating beams in both on- and off-axis orientation. All NBI deuterons have 1.0 MeV initial energy.
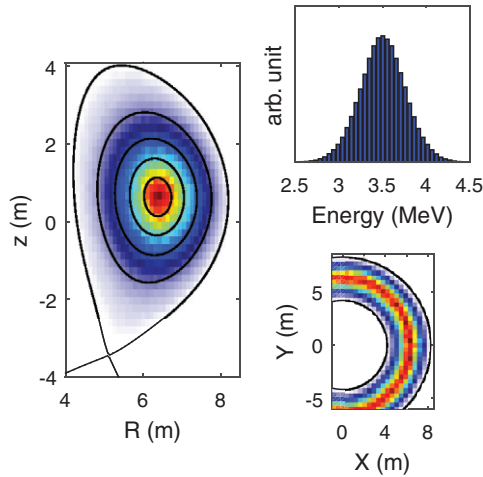
Figure 8. The initial test particle distribution of thermonuclear alpha particles in the **flat top** phase. The alpha particles have uniform distribution in pitch ξ.

location, facilitating even direct orbit losses in the plasma periphery. Furthermore, the alphas are born with three times higher mean energy than the NBI ions. This translates into larger gyro-radii and orbit widths. Both of these contribute to faster transport of fusion alphas and, consequently, larger wall power loads.

The good confinement of the energetic ions even in the presence of TBMs is further reflected in their slowing-down density profiles. The flux surface averaged fast ion density, displayed in figure 10 for simulations with and without TBMs, shows only minor differences. The safety factor $q = 1$ for the flat top phase is situated near $\rho_{\text{pol}} = 0.55$. The TBM slightly increases the magnetic island present at that location, which causes a visible local modification to the NBI density. There is also variation in the density near the magnetic axis. There the poloidal component of the plasma equilibrium magnetic field vanishes. This allows even a weak perturbation field to affect the fast ion confinement.

Even though the total power to the wall is small, before we can claim that the TBMs can be safely employed in ITER, the *distribution* of this power on the wall also has to be investigated to identify the existence of possible hot spots that could lead to first wall damage. If two simulations are to be compared quantitatively, it is best to study one-dimensional line plots. With the asymmetric first wall, producing such a
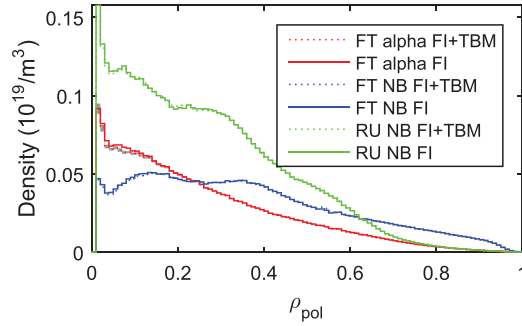
beam ions are co-injected into well-confined banana orbits, while one has no control over the orbits on which the alphas are born. Due to their isotropic birth velocity distribution, half of the alphas will have their velocity in direction opposite to the plasma current and, thus, are born on orbits where the gradient drift will take them outward from their birth
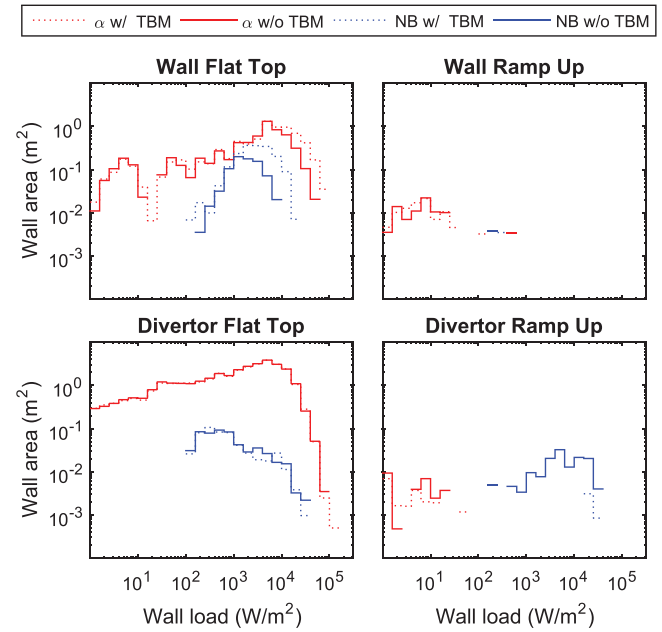
Figure 10. The slowing-down density profile of fast partices in the various simulations. The TBMs cause no significant changes in the profiles. The shaded area depicts the one standard deviation Monte-Carlo noise confidence interval for the flat top with TBM case. It was calculated with the *standard error of the mean* formula by splitting the simulation into 10 smaller simulations.


Figure 11. The wall area receiving a given power load. The alpha particle wall loads have wider spectrum than the NBI deuterons. This is due to a difference in the weighting schemes: the alpha particle weights (i.e. how many real particles a test particle represents) vary depending on the value of the fusion reactivity at the birth location, so the power they carry to the wall has a wide range of variation; in contrast, all the NBI test ions carry equal weight, so the power load they produce has much smaller variation. The mean area of the wall elements is approximately $25 \, cm^2$ ($10^{-2.6}$ m^2) and the wall total area is 890 m^2.

plot requires careful analysis. Toroidal or poloidal averages naturally remove details. The method we chose is a novel one: The distribution of the power deposited to the wall by fast ions is analysed by calculating a histogram of the power loads. Each wall element contributes its area to a bin defined by the power load the element receives (figure 11).

For the flat top phase, the TBMs increase the wall area receiving more than one kW m^{-2}. The high power load tail extends to higher wall loads with the TBMs: for alphas the tail extends to $10^{4.8}$ (about 63 000) W m^{-2} without TBMs and $10^{5.0}$ W m^{-2} with TBMs. A similar effect is seen also for the neutral beam ions. This would imply larger, more intensive hot spot(s). There is almost no change in the divertor loads, implying that the wetted area hasn't changed nor has the power changed. There is no clear trend visible for the ramp-up phase. This indicates that there is no significant effect from the TBMs. The wall loads must, however, be further analysed visually. Since the ramp-up phase exhibits vanishingly low power loads to the wall, we shall concentrate on the flat top phase.

Figure 12 shows the wall distribution of the power load in the FT phase. The wall structure displayed in figure 5 is flattened on the plane spanned by the toroidal and poloidal angles. In the flattened case, also the statistical significance is indicated by the saturation of the color. The power load was calculated simply by summing up the power carried by the particles hitting the wall elements and then dividing by the element surface area. The statistical significance of the power load values was assessed by calculating the one standard deviation confidence interval with 250 bootstrap samples of the test particle ensemble. In the figure 12, the colors are fully unsaturated (white) if the one-sided confidence interval exceeds 80% of the power, and fully saturated when the interval is less than 50% of the power. For the ramp-up phase, the loads are small and the significance is low, so they are not presented graphically.

Figure 13 shows the toroidal distribution of the alpha power loads near the equator at low field side. Increased losses are observed not only in the vicinity of the TBMs but also near the NBI ports. This is understandable because the ferritic inserts there are modified to accommodate the beam

ducts. The space for ferritic inserts is restricted at those ports, and, therefore, the TF coil ripple is not mitigated as effectively as for the rest of the device (see figure 1). However, no new hot spots are introduced by the TBMs. Instead of that, the additional load intensifies the power deposited to already heated areas.

3.3. Analysis of the ions lost to the wall and divertor

It is of interest to try to find where in phase space the particles hitting the wall originate from and what kind of process may be responsible for their escape from the plasma. ASCOT stores both the initial and final phase space coordinates for all test particles, making it possible to identify the birth regions of particles contributing to the wall load. In our analysis, the lost ions are categorized into ten groups. First they are grouped into prompt and diffusive losses by their flight time. (The word diffusive is used here to denote the relatively slow random walk like process producing transport of ions. Possible causes include collisional scattering, magnetic field stochasticity and banana tip drift. The code cannot separate the effects.) For both type of losses the ions are categorized according to the part of the wall they hit. In the case of diffusive losses, hits near the equator are further categorized by their final pitch angle, with particles having a final pitch $\xi = v_{\parallel}/v_{tot} < 0.2933$ labelled as 'ripple trapped' (i.e. ions trapped in between to adjacent field coils. The ripple well in these backgrounds
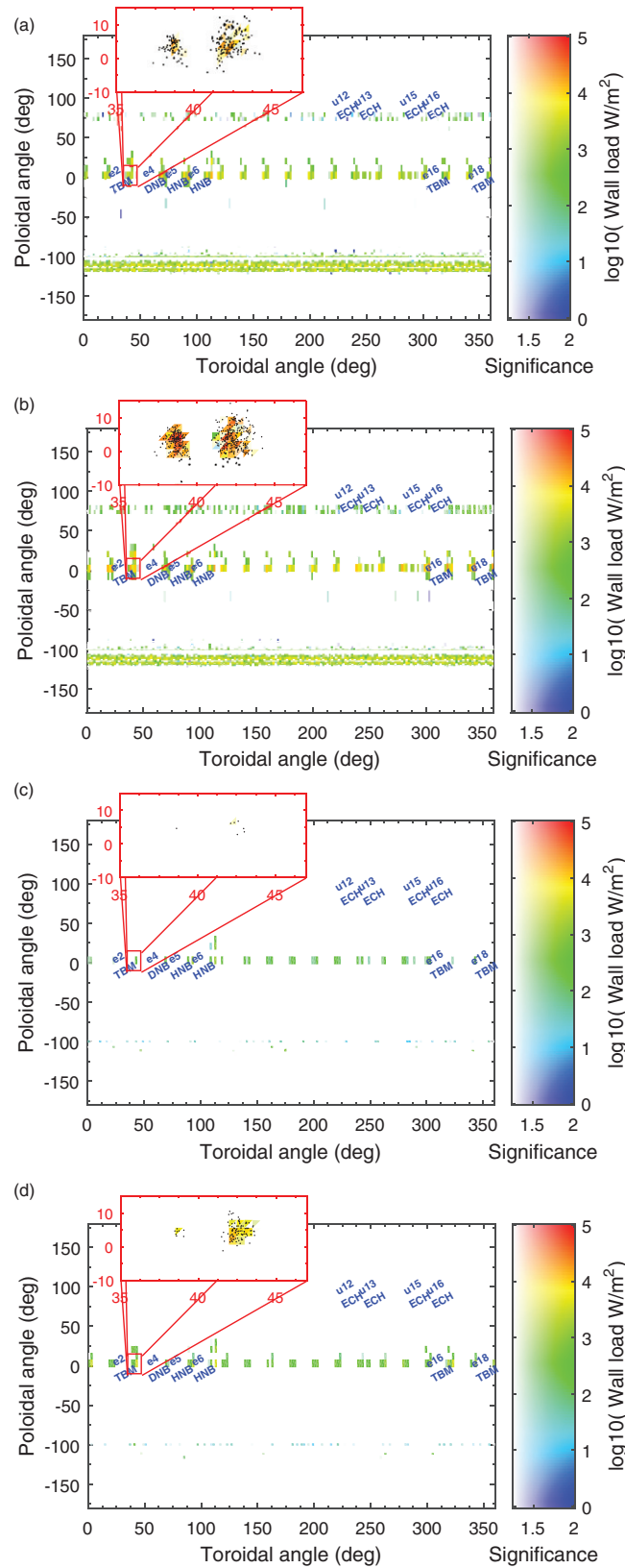
Figure 12. The wall power loads in the **flat top** phase for thermonuclear alphas (*a*) and (*b*) and for NBI ions (*c*) and (*d*). The odd rows (*a*) and (*c*) show the results for cases without TBMs and the even rows (*b*) and (*d*) for cases with TBMs. The wall shown in figure 5 is unfolded onto a plane. The hue and saturation of the wall element color depicts the power load and its statistical significance, respectively. The insert shows the power load calculated using the original detailed wall. The fast ion hit locations are indicated with black dots. The larger image shows wall loads where 32 triangles have been combined into a rectangle before calculating the power load.
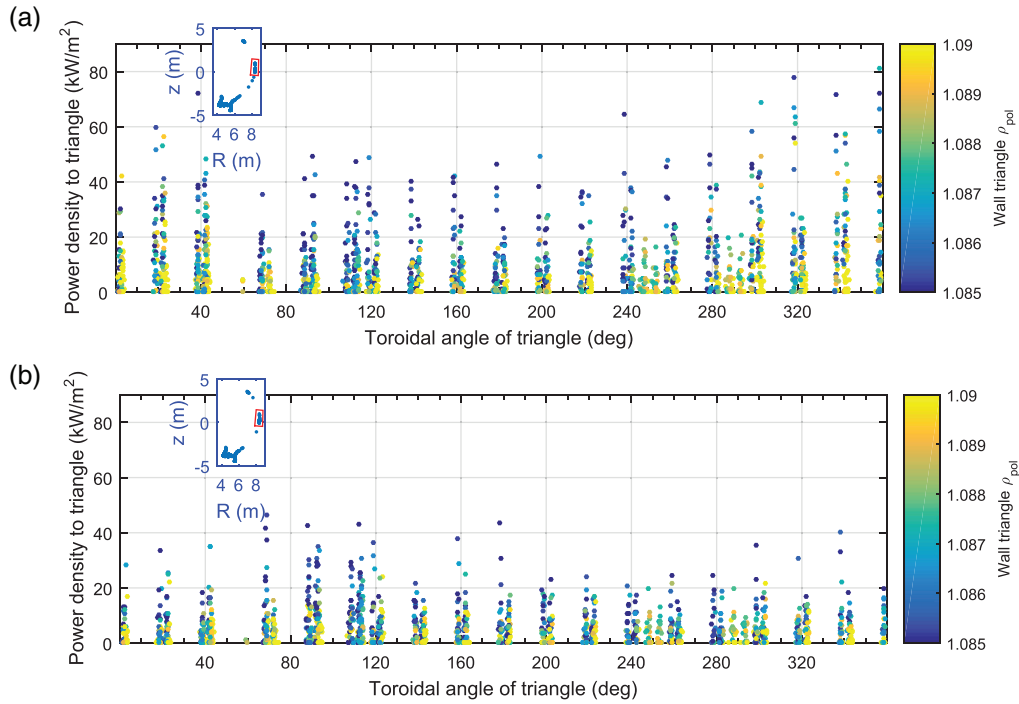
Figure 13. The alpha wall power loads near magnetic midplane at the low field side with (*a*) and without (*b*) the TBMs for the flat top phase. The red quadrangle in the insert depicts the analysed poloidal area. In the main graph, each wall triangle is depicted with a dot. The colouring depicts the radial coordinate of the wall tile.

Table 2. Analysis of the wall power load due to fusion alphas in the flat top phase of the 15 MA scenario.

		With TBMs	Without TBMs
prompt	wall	2.4 kW	2.2 kW
	outer divertor	30 kW	30 kW
	inner divertor	19 kW	20 kW
	divertor dome	41 kW	40 kW
diffusion	outer divertor	6.0 kW	5.8 kW
	divertor dome	15 kW	15 kW
	inner divertor	16 kW	16 kW
	equator	3.1 kW	2.1 kW
	upper port	5.7 kW	2.4 kW
	ripple trapped	55 kW	27 kW

Note: The losses are determined 'prompt' or 'diffusive' based on the time it takes them to reach the wall. See the text.

is too shallow to directly bring particles to the wall, but it can still enhance banana transport by transiently trapping particles.)

The alpha power that each category delivers in the flat top phase is shown in table 2. Figure 14 shows the distribution of the power carried by the alphas to the wall and divertor as a function of three different quantities: the flight time, i.e. the time it takes them to reach the wall, their initial minor radius ρ_{pol} coordinate and their pitch ξ at wall collision. The TBMs produce only minor changes in the prompt losses. The field perturbations caused by the TBMs are too small to significantly change the short trajectories of the prompt losses. Even at diffusion time scale the divertor power is nearly unaffected. However, TBMs cause

a noticeable increase in wall power. This is in agreement with simulation results of thermal ions [26] and could be due to the increased ripple diffusion of the banana orbits. The TBMs do not only increase the flux of particles from the edge, but of particles arriving from deeper in the plasma as well (figures 14(*c*) and (*d*)). If the banana ripple diffusion is the main transport mechanism due to the TBMs, it is natural that the divertor loads are unaffected: divertor hits are predominantly from passing particles. At slowing down time scale (0.1–1 s) the power is deposited mainly to the low field side equator (ripple losses), near the upper ports and also to the divertor dome. The wall losses are increased by the TBMs.

The ions in the *Equator* and *Upper port* categories have the widest orbits, i.e. they are marginally trapped bananas. They pass nearest to the FIs and TBMs and have largest diffusion steps (i.e. banana widths). Hence, they are most susceptile for the perturbations due to the TBMs.

A similar analysis for the lost NBI deuterons was not carried out because the co-injected beam ions are born with a narrow distribution of initial pitches, putting them on well-confined orbits. Furthermore, only very few of the NBI deuterons are ionized where they could be lost.

4. Summary and discussion

According to the presented ASCOT simulations, ITER fast ion confinement is not compromised by the European test blanket modules in the *15 MA Q = 10 inductive scenario*. This was tested for both thermonuclear alphas and NBI ions. While the wall loads due to the fast ions were generally increased by the TBMs, they remained at the level of tens to a hundred kW.
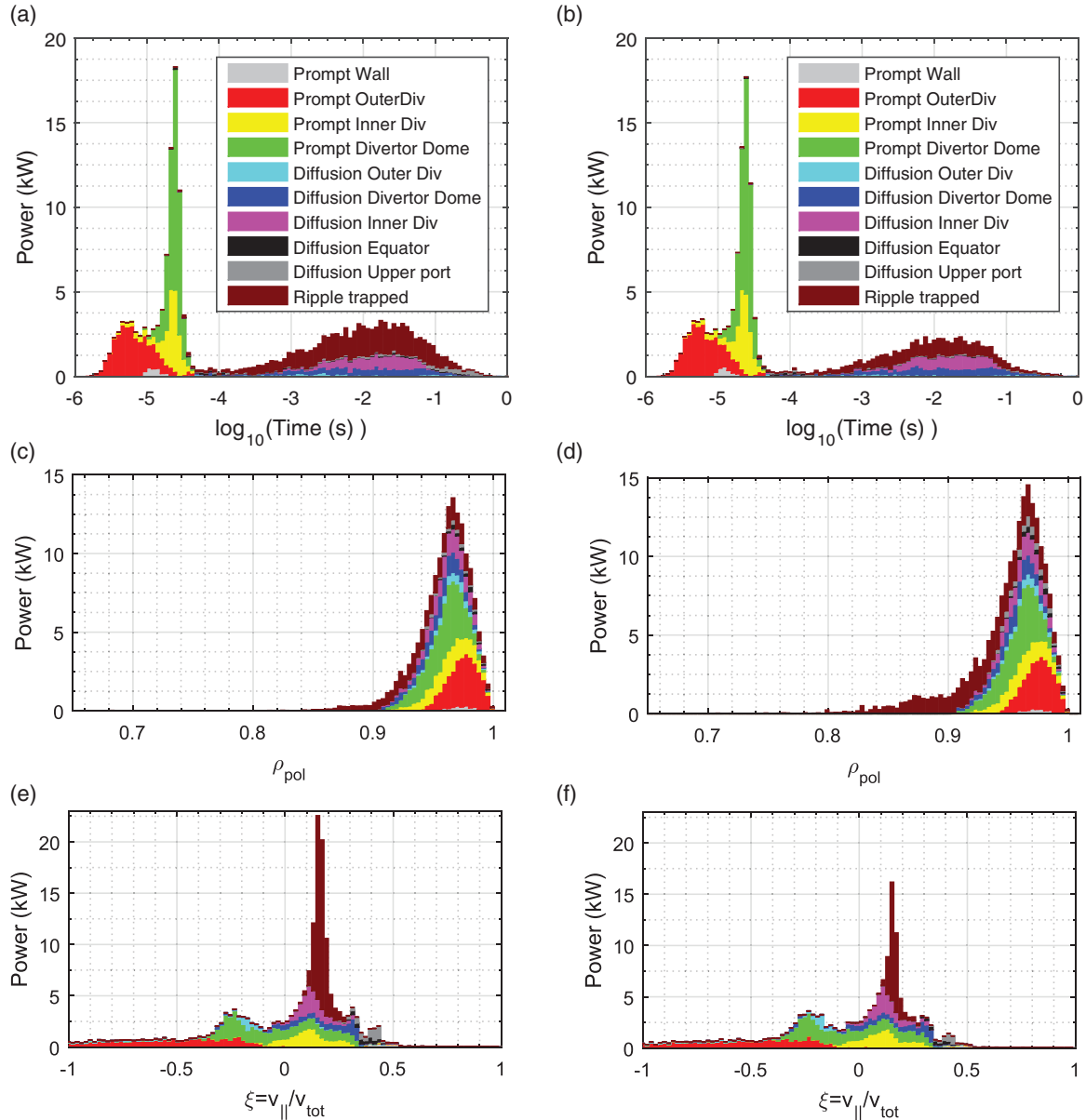
Figure 14. Analysis of the flat top phase alpha power lost to the wall with (*a*), (*c*) and (*e*) and without (*b*), (*d*) and (*f*) the TBMs' contribution to the magnetic field. The different colors of the stacked histograms indicate division of the power to various loss mechanisms. The ordinate shows the amount of power that each bin delivers to the wall. The abscissa depicts (*a*) and (*b*) the time from fusion to wall hit on logarithmic scale, (*c*) and (*d*) the initial minor radius (ρ_{pol}) coordinate of the particles, and (*e*) and (*f*) the pitch of the particles when hitting the wall.

The increase is attributed to ions born slightly deeper in the plasma that the TBM perturbation allows to get lost. However, no evidence for non-diffusive channelling of fast ions, possibly leading to hot spots, was found but, instead, the diffusive loss channels were intensified.

There are, however, a couple of caveats that could affect these conclusions. The ICRH ions were not included in this study. As a first approximation they can be considered as ions on very wide banana orbits with high energy. Such particles naturally occur in our fusion alpha simulations, which suggests that the presence of ICRH would not dramatically change the results of this article. Nonetheless, a rigorous ICRH study will be commenced once the proper ICRH source has been implemented in ASCOT. Another

shortcoming of this analysis is related to the plasma response to the 3D magnetic field. A rotating plasma is expected tor respond to the non-axisymmetric vacuum magnetic field, but there are large uncertainties in the rotation of the ITER plasma. The magnetic fields used in this study correspond to the limit of toroidally slowly rotating ITER plasma, the 'vacuum approximation', where plasma neither shields the pitch resonant field components nor amplifies them through the kink response [27, 28]. If the resonant components do penetrate, they tend to brake the rotation, thus further reducing the plasma shielding [29]. On the other hand, the amplification of the non-resonant components may compensate the effect of the shielding [30]. Also magnetohydrodynamic modes such as Alfvén eigenmodes, tearing modes and

edge localized modes can affect the fast ion losses. However, addressing the MHD-related issues will require close collaboration with MHD experts. Work in this direction has already started.

Acknowledgments

References

[1] Salavy J.F., Boccaccini L., Chaudhuri P., Cho S., Enoeda M., Giancarli L., Kurtz R., Luo T., Rao K.B.S. and Wong C. 2010 *Fusion Eng. Des.* **85** 1896

[2] Kramer G. *et al* 2011 *Nucl. Fusion* **51** 103029

[3] Hirvijoki E., Asunta O., Koskela T., Kurki-Suonio T., Miettunen J., Sipilä S., Snicker A. and Äkäslompolo S. 2014 *Comput. Phys. Commun.* **185** 1310

[4] Kurki-Suonio T. *et al* 2009 *Nucl. Fusion* **49** 095001

[5] Snicker A., Kurki-Suonio T. and Sipilä S. K. 2010 *IEEE Trans. Plasma Sci.* **38** 2177

[6] Kramer G. *et al* 2013 *Nucl. Fusion* **53** 123018

[7] Chen Y., Feng K., Gao C. and Zhang G. 2011 *Fusion Eng. Des.* **86** 2273

[8] Liu S., Liu Y., Wang W., Lu R., Jin M. and Zeng Q. 2009 *Fusion Eng. Des.* **84** 1206

[9] Chen Y., Feng K., Gao C., Zhang G. and Li Z. 2010 *Fusion Eng. Des.* **85** 2150

[10] Aymar R., Barabaschi P. and Shimomura Y. 2002 *Plasma Phys. Control. Fusion* **44** 519

[11] Fasoli A. *et al* 2007 *Nucl. Fusion* **47** S264

[12] Mimata H., Tani K., Tobita K., Tsutsui H., Tsuji-Iio S. and Shimada R. 2008 Progress in nuclear energy *Innovative Nuclear Energy Systems for Sustainable Development of the World. Proc. of the Second COE-INES Int. Symp. INES-2* (*Yokohama, Japan*, *26–30 November 2006*) vol 50 p 638

[13] Snicker A., Sipilä S. and Kurki-Suonio T. 2012 *Nucl. Fusion* **52** 094011

[14] Hirvijoki E., Brizard A., Snicker A. and Kurki-Suonio T. 2013 *Phys. Plasmas* **20** 092505

[15] Gagliardi M. 2012 *F4E-GRT-379 Data Pack 1* F4E_D_25MJJ6

[16] Äkäslompolo S., Asunta O., Bergmans T., Gagliardi M., Galabert J., Hirvijoki E., Kurki-Suonio T., Sipilä S., Snicker A. and Särkimäki K. 2015 Calculating the 3D magnetic field of ITER for European TBM Studies *Fusion Eng. Des.* in press doi:10.1016/j.fusengdes.2015.05.038

[17] Liu Y.Q., Bondeson A., Fransson C.M., Lennartson B. and Breitholtz C. 2000 *Phys. Plasmas* **7** 3681

[18] Huysmans G. and Czarny O. 2007 *Nucl. Fusion* **47** 659

[19] Parail V. *et al* 2013 *Nucl. Fusion* **53** 113002

[20] Gagliardi M. 2012 *F4E-GRT-379 Data Pack 2* F4E_D_252PBZ

[21] Äkäslompolo S. *et al* 2012 *39th EPS Conf. on Plasma Physics 16th Int. Congress on Plasma Physics (Europhysics Conference Abstracts vol 36F)* ed S. Ratynskaya *et al* P5.058, http://ocs.ciemat.es/epsicpp2012pap/pdf/P5.058.pdf

[22] Bosch H.S. and Hale G. 1992 *Nucl. Fusion* **32** 611

[23] Brysk H. 1973 *Plasma Phys.* **15** 611

[24] Asunta O., Govenius J., Budny R., Gorelenkova M., Tardini G., Kurki-Suonio T., Salmi A., Sipilä S., the ASDEX Upgrade Team and the JET EFDA 2015 *Comput. Phys. Commun.* **188** 33

[25] Suzuki S., Shirai T., Nemoto M., Tobita K., Kubo H., Sugie T., Sakasai A. and Kusama Y. 1998 *Plasma Phys. Control. Fusion* **40** 2097

[26] Oyama N., Urano H., Shinohara K., Honda M., Takizuka T., Hayashi N., Kamada Y. and The JT-60 Team 2012 *Nucl. Fusion* **52** 114013

[27] Liu Y., Kirk A., Gribov Y., Gryaznevich M., Hender T. and Nardon E. 2011 *Nucl. Fusion* **51** 083002

[28] Haskey S.R., Lanctot M.J., Liu Y.Q., Hanson J.M., Blackwell B.D. and Nazikian R. 2014 *Plasma Phys. Control. Fusion* **56** 035005

[29] Kirk A., Harrison J., Liu Y., Nardon E., Chapman I. and Denner P. 2012 *Phys. Rev. Lett.* **108** 255003

[30] Pfefferlé D., Misev C., Cooper W.A. and Graves J. P. 2015 *Nucl. Fusion* **55** 012001